Influence of passivation, doping and geometrical parameters on the avalanche breakdown of GaN SBDs

B. Orfao[1], R. A. Peña[2], B. G. Vasallo[2], S. Pérez[2], J. Mateos[2] and T. González[2]

[1] CNRS-IEMN, Université de Lille, UMR8520, Av. Poincaré, 59650 Villeneuve d'Ascq, France
[2] Applied Physics Department and USAL-NANOLAB, Universidad de Salamanca, 37008 Salamanca, Spain

E-mail: beatriz.orfao-e-vale-tabernero@univ-lille.fr

Abstract

The breakdown of GaN-based Schottky barrier diodes associated with impact-ionization events initiated by electrons injected by tunneling is physically analyzed by means of a Monte Carlo simulator self-consistently coupled with a two-dimensional solution of the Poisson equation. Simulations of a realistic topology where different geometrical parameters are modified allow to identify their influence on the breakdown voltage. The correct physical modelling of two-dimensional effects is essential for a proper prediction of the breakdown. Epilayer doping and thickness, dielectric used for the passivation and lateral extension of the epilayer are analyzed. As expected, the lower the doping and the thicker the epilayer, the higher the value found for the breakdown voltage, but, interestingly, the results also indicate that the peak electric field present at the edge of the Schottky contact, which may be reduced by means of high-k dielectric passivation and a short lateral extension of the epilayer, plays a key role in the breakdown.

Keywords: Schottky barrier diode, impact ionization, tunnel current, breakdown

1. Introduction

In the last years, GaN has generated an increased interest due to its properties such as wide bandgap, high mobility, high breakdown field and high electron saturation velocity[1], which makes it suitable for high frequency and high-power applications [2]. Presently, THz and sub-THz electronic sources rely on frequency multipliers based in the classic GaAs Schottky Barrier Diode (SBD) technology[3,4], but the output power at frequencies above 500 GHz is limited by the low breakdown voltage and the small size of the diodes (necessary to be used at high frequencies) [5]. Apart from complex designs including multiple diodes, exploiting the "power-combining" circuit topology [6,7], the use of GaN SBDs can potentially increase the RF power output level at the intermediate stages of frequency-multiplied sources. Indeed, the key parameter for weighting the power performance of GaN SBDs is their breakdown voltage, which is theoretically much higher than that of GaAs-based diodes [8,9]. However, the diode breakdown mechanism is not only related to the semiconductor properties, but it is also intimately linked to the presence of a reverse leakage current, problem widely studied in GaN SBDs and partially mitigated by recent technological advances. The presence of trap-related mechanisms such as trap-assisted tunneling, Poole Frenkel emission or variable range hopping [10-12] leads to a higher leakage current in comparison with the expected ideal one, which includes thermionic emission and tunneling contributions [13,14]. This problem can be very significant in non-mature technologies such as GaN SBDs, but the use of native GaN substrates instead of foreign ones (SiC, Si or sapphire) allows mitigating the excess leakage current by presenting a lower density of defects in the semiconductor, which improves the Schottky contact quality [15].

The electric field crowding effect at the edge of the junction also provokes an increase of the leakage current that could lead to premature breakdown [16]. Indeed, the high values of the electric field appearing at the metal-semiconductor interface enhance the electron injection by tunneling [17]. Thus, a breakdown voltage improvement could be achieved by using dielectric passivation, which smooths the electric field at the contact edges [18]. A correct physical modelling of all the involved processes is essential in the analysis of the breakdown. In particular, electron and hole impact ionization (II) processes produced by tunneled electrons should be considered when analyzing the reverse leakage current because they are, together with the high electric fields at the contact edges, at the origin of the avalanche breakdown in SBDs [19]. Additionally, the barrier profile should be self-consistently calculated with the carrier concentration in the depletion region, since the full-depletion assumption may be no longer valid [20].

In this work, the role played by II in the breakdown voltage of SBDs has been physically studied through a homemade semiclassical ensemble Monte Carlo (MC) simulator coupled with a two-dimensional (2D) Poisson's equation solver [20-22]. The influence of different technological parameters on the breakdown voltage will be qualitatively analyzed, as the dielectric passivation material, the epilayer doping level, and the epilayer thickness and lateral extension from the Schottky contact. The paper is organized as follows. The simulated structure of the diodes and the MC model are described in Sec. 2. The results and their discussion are reported in Sec. 3. Finally, the main conclusions are drawn in Sec. 4.

2. Physical model and simulated structure

The ideal current mechanisms in SBDs are thermionic emission and tunnel injection. The tunnel injection becomes more relevant for reverse bias. To determine these current contributions, it is necessary to know the barrier profile along the structure. To calculate the tunneling current at a given energy ε, we use the general expression:

$$J(\varepsilon)d\varepsilon = -eN(\varepsilon)T_C(\varepsilon)d\varepsilon, \qquad (1)$$

where $N(\varepsilon)$ is the number of electrons per unit area incident on the barrier with an energy ε per unit time and per unit energy and $T_c(\varepsilon)$ is the transmission coefficient. This expression assumes that the occupation of the final states is negligible. For solving the Schrodinger equation, we have used the Wentzel-Kramers-Brillouin (WKB) approximation, obtaining that T_c is equal to [23]:

$$T_C(\varepsilon) = exp\left(-\frac{2}{\hbar}\int_{x_1}^{x_2}\sqrt{2m^*(\varepsilon_c(x)-\varepsilon)}dx\right), \qquad (2)$$

being $\hbar$ the Planck constant, m^* the electron effective mass, and x_1 and x_2 the two classical turning points for the potential barrier. In the MC simulator, a region where the tunnel injection takes place is defined. T_c is calculated for each energy interval in which the conduction band is discretized. At each of these intervals, the details of injected charge are determined: number of injected particles, and time and position at which they are injected [24]. As in [13,20], we have considered the exact expression of $N(\varepsilon)$, including transversal states [25]:

$$N(\varepsilon) = \frac{A^*T}{ek_B} ln\left[1 + exp\left(-\frac{\varepsilon-\varepsilon_F}{k_BT}\right)\right], \qquad (3)$$

where A^* is the Richardson constant, T the temperature, k_B the Boltzmann constant, e the electron charge and ε_F the Fermi energy.

The GaN conduction band model used for electrons in our MC simulator consists of three non-parabolic spherical valleys, Γ_1, (6 equivalent) U and Γ_3 [26]. Carriers are subjected to scattering mechanisms, which are randomly selected according to their respective probabilities. The mechanisms considered in the simulations include intervalley scattering, phonon scattering (acoustic and polar, both optical and non-optical), ionized impurity scattering, and piezoelectric scattering. The probabilities of these mechanisms, as well as the final carrier states, have been previously studied in detail [26,27]. The parameters and scattering mechanisms of electrons in the conduction band are the same as in [27], summarized in Table I. The MC model for holes in the valence band consists of only one valley globally representing heavy, light, and split-off bands. The hole parameters have been adjusted by comparison with the three-valley model used in [20].

TABLE I. SIMULATION PARAMETERS FOR GAN AND ELECTRON TRANSPORT

Parameter	GaN		
Density (kg/m^3)	6150		
Sound velocity (m/s)	6560		
Optic dielectric constant	5.35		
Static dielectric constant	8.9		
Optical phonon energy (eV)	0.09120		
Band gap (eV)	3.44		
Lattice parameter (Å)	5.185		
	Γ_1	U	Γ_3
Effective mass (m^*/m_0)	0.22	0.39	0.28
No parabolicity coef. (eV^{-1})	0.37	0.50	0.22
Energy from Γ valley	0.0	2.2	2.4
Acoustic def. pot. (eV)	8.3	8.3	8.3
Optic def. pot. (eV)	0.0	0.0	0.0
Intervalley def. pot. (10^{10} eV/m)			
From Γ_1 to	0	10	10
From U to	10	10	10
From Γ_3 to	10	10	0
Intervalley phonon energy (eV)			
From Γ_1 to	0	0.09120	0.09120
From U to	0.09120	0.09120	0.09120
From Γ_3 to	0.09120	0.09120	0

For high reverse bias conditions, in addition to tunnel injection, II events should be considered for both electrons and holes. II may occur when electrons in the conduction band have an energy exceeding a threshold value ε_{th}, resulting in the generation of an electron–hole pair. This phenomenon has been introduced in the simulator as an additional scattering mechanism using the Keldysh approach, under which the probability per unit time of having an II event is given by the following expression [28,29]:

$$P(\varepsilon) = S\left(\frac{\varepsilon-\varepsilon_{th}}{\varepsilon_{th}}\right)^2 \qquad if \quad \varepsilon > \varepsilon_{th}$$
$$P(\varepsilon) = 0 \qquad if \quad \varepsilon < \varepsilon_{th} \qquad (4)$$

being ε the carrier kinetic energy, ε_{th} the ionization threshold energy (3 eV for both electrons and holes) and S the softness or hardness of the threshold (5×10^{12} s^{-1} for electrons and 25×10^{12} s^{-1} for holes). The generated carriers appear in the lower-energy valleys, since these are the most probable to be occupied. The electron that produces the II event remains in the valley where it is located, losing an energy equivalent to the sum of the bandgap and the thermal energy transferred to the electron–hole pair. For high reverse bias, II phenomena may provoke a sharp increase of the current, eventually leading to the diode breakdown. In our simulations, the breakdown is identified by the inability to reach a steady-state condition due to the indefinite increase in the number of carriers, which is usually accompanied by a previous sharp growth of the current.

Surface charges present at the dielectric-semiconductor interface, inducing carrier depletion through Coulomb repulsion, are also included in the simulation. Local values of surface-charge density σ are self-consistently calculated with the number of carriers present near the interface [18]. In this way, σ is consistent with the electron distribution for each bias condition and adapted to the geometry of every structure.

The MC models used in this work (carrier transport, II processes, surface-charge at the interfaces, tunnel injection, etc.) have already been validated in previous studies on other devices [20-22,24,27,28].

The simulated device, based on real planar GaN SBDs, consists of a highly doped n^+ substrate with doping $N_s=5\times10^{18}$ cm^{-3}, and a n^- epilayer with doping N_D, whose influence on the breakdown conditions is analysed. The Schottky contact length, L_{Sch}, is 200 nm. Figure 1 shows a scheme of the complete 2D topology. The red dashed rectangle delimits the one-dimensional (1D) diode corresponding to the vertical region under the Schottky contact, which will be also simulated for comparison. The epilayer thickness W_{EP} and lateral extension from the Schottky contact L_{EP} are also magnitudes under study. The surface charges σ located at the dielectric–semiconductor interface are represented by a violet line. As mentioned, besides N_D, W_{EP} and L_{EP}, we will study the influence on the breakdown performance of the

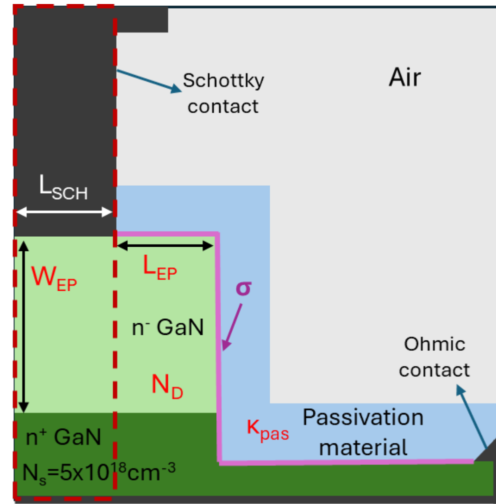

Figure 1. Scheme of the simulated SBDs. The red dashed rectangle indicates the 1D diode structure. A study of the device breakdown is carried out with respect to the parameters: N_D, W_{EP}, L_{EP} and κ_{pas}.

passivation material, characterized by its dielectric constant κ_{pas}. The breakdown voltage can be improved by the presence of a passivation dielectric, as it smooths the sharp potential drop at the edges of the Schottky contact, an effect previously reported in [18]. To ensure the accuracy of the simulations, a time step Δt=0.2 fs is considered for a total time of 40 ps. The device mesh discretization has been done by using rectangular cells of 2–5 nm sides, smaller than the Debye length in the considered semiconductor.

3. Results and Discussion

In this section, the influence on the breakdown voltage of the different geometrical parameters (κ_{pas}, N_D, W_{EP} and L_{EP}) will be analyzed in detail.

3.1 Passivation

In order to study the influence on the breakdown voltage of the dielectric passivation material, simulations for a 2D structure with $N_D=3\times10^{17}$$cm^{-3}$, W_{EP}=350 nm, L_{EP}=200 nm, and without (κ_{pas}=1) and with high-k dielectric passivation (κ_{pas}=25) were carried out. The resulting I-V curves in reverse bias, considering and not II, are shown in figure 2. In the absence of II, the current smoothly increases following the ideal tunneling behaviour. However, II events lead to a sharp increase of the current appearing for high reverse bias and thus to the avalanche breakdown of both diodes, which is identified by the fact that a stationary situation is not reached in the simulation due to a progressive increase of the carrier number and, as consequence, of the current. Thus, the inclusion of II events and hole transport in the simulations is essential to understand and optimize this physical behaviour.

To further evidence the influence of the passivation layer (air or a high-k material) and the associated 2D effects on the

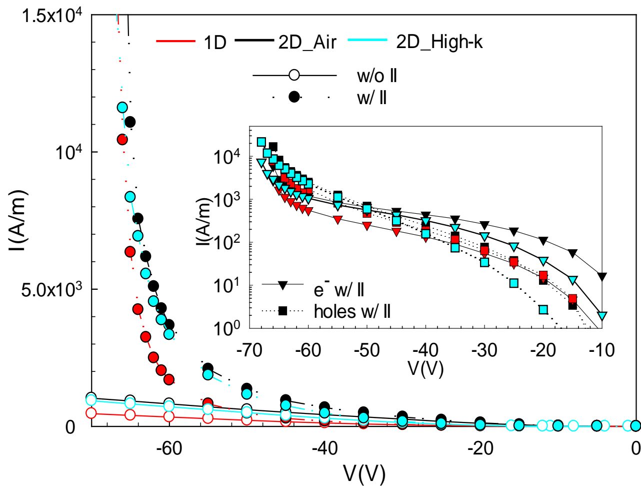

Figure 2. *I-V* curves of the 2D structure of figure 1 (with N_D=3x10^{17}cm^{-3}, W_{EP}=350 nm, L_{EP}=200 nm) calculated with (close circles) and without (open circles) including II events in the simulation, with air (black) or a high-k dielectric (cyan) considered as dielectric. Inset: Electron (triangles) and hole (squares) current contributions. The case of a 1D structure (consisting of just the vertical region under the Schottky contact) is also shown in red for comparison.

avalanche breakdown, simulations of a 1D structure, consisting of the vertical diode delimited by the red-dashed line in figure 1, were carried out. The increase of the current when increasing the reverse bias is more pronounced in the 2D structures due to the enhanced electric field at the edge of the Schottky contact [18], not present in the 1D case, which leads to intense II events in the neighbouring region.

Besides, the higher the permittivity of the passivation material, the lower the value of the electric field peak found at the edge of the Schottky contact [18], and thus the lower the value of the current achieved when considering II. This is evident when the reverse bias is lower than 40 V, above that voltage the current is similar for both non-passivated and passivated SBDs, which indicates that the influence of 2D effects is reduced. This occurs because, even if the peak electric field at the edge is still slightly different, the contribution along the whole Schottky contact becomes more relevant than just the high value at the edge.

The MC simulator allows us to distinguish between two current contributions, considering the number of carriers that reach the Schottky contact: one associated with electrons (tunnel injection) and the other one associated with holes (coming from II events). These two contributions are represented in the inset of figure 2. For the lower voltages, the hole current contribution is negligible. As the bias is increased, it becomes comparable to the electron contribution, and finally, for the higher voltages (just before the appearance of the avalanche breakdown), it becomes dominant. The breakdown is explained as a consequence of II as following. For high enough voltages, II leads to an increasing presence of carriers at the vicinity of the Schottky contact, which in turn provokes an increase of the electric field (mainly at the

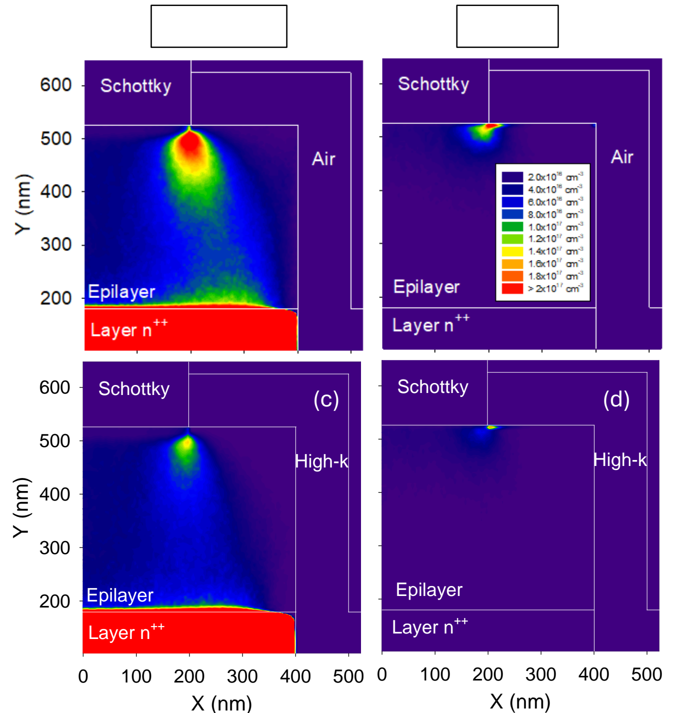

Figure 3. Colour maps of (a) and (c) electron and (b) and (d) hole concentrations for N_D=3x10^{17}cm^{-3}, W_{EP}=350 nm, L_{EP}=200 nm and an applied voltage of -35 V with (a) and (b) air and (c) and (d) high-k as dielectric material.

contact edge), with the subsequent enhancement of electron injection by tunneling. Consequently, more II events take place, ultimately leading to the breakdown of the diode.

Figure 3 presents color maps of electron and hole concentration considering air and high-k as dielectric passivation materials for an applied voltage of -35 V, when II is evident but far enough from the avalanche breakdown. For the bias represented in the figure the epilayer is almost fully depleted. As observed, the tunnel injection is located at the edge of the Schottky contact, being more pronounced when the diode is not passivated. As mentioned previously, the electric field is stronger at the contact edge, leading to the appearance of II events and therefore to the presence of a non-negligible hole concentration. As the electric field peak is reduced when the dielectric permittivity increases, also the hole current contribution (inset of figure 2) is lower due to both the lower electron injection and the less frequent II events.

3.2 Epilayer doping and Thickness

The second technological parameter we have studied is the epilayer doping level N_D. Simulations of the 2D structure with W_{EP}=350 nm, L_{EP}=200 nm, and without passivation (κ_{pas}=1) were performed for three different values of N_D: 10^{17}, 3×10^{17} and 6×10^{17} cm^{-3}. Note that the values of W_{EP}, L_{EP} and κ_{pas} are not the optimal ones in terms of the breakdown behaviour. However, these values allow to more clearly identify the

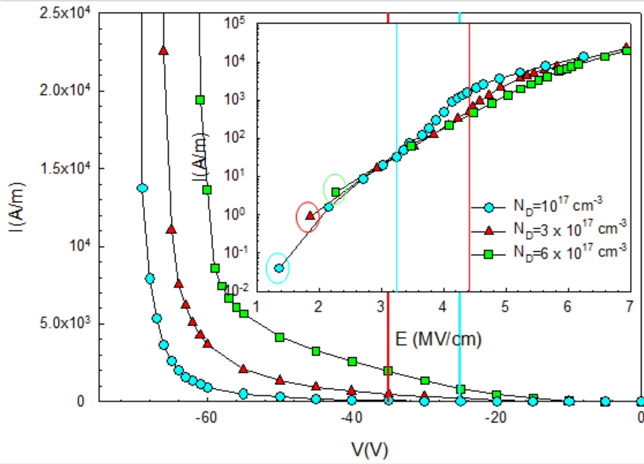

Figure 4. Simulated *I-V* curves obtained for a 2D structure with W_{EP}=350 nm, L_{EP}=200 nm and different epilayer doping levels: N_D=10^{17} (cyan), 3x10^{17} (red) and 6x10^{17} cm^{-3} (green). Inset: Current as a function of the electric field at the edge of the Schottky contact (the symbols sorrounded by circles correspond to an applied voltage of -5V). The vertical lines indicate the condition for which a total epilayer depletion is found in the simulations.

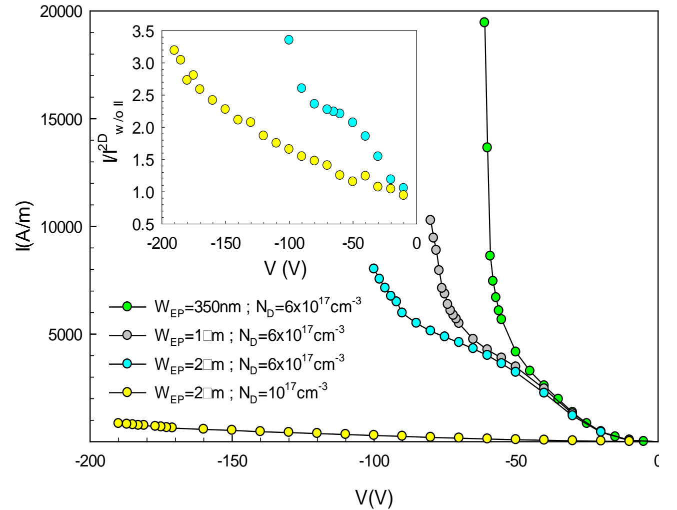

Figure 5. Simulated *I-V* curves obtained for diodes with N_D=6x10^{17} cm^{-3}, L_{EP}=200 nm and different epilayer thickness: W_{EP}=350 nm (green), 1 µm (grey) and 2 µm (cyan); and a diode with N_D=10^{17} cm^{-3}, L_{EP}=200 nm and W_{EP}=2 µm (yellow). The inset shows the ratio of the current values obtained with and without considering II processes in the simulation for the diodes with an epilayer thickness of 2 µm.

influence of N_D. In particular, such small value of W_{EP}, while useful for high-frequency applications, leads to a reduction of the breakdown voltage as will be shown later. In figure 4, the corresponding *I-V* characteristics are represented. As observed, the breakdown voltage lies in the range 60-70 V, being lower when the doping is increased due to the higher electric field present at the contact for the same bias, which leads to a higher tunnel injection.

The breakdown for diodes with W_{EP} =350 nm is strongly linked to the full depletion of the epilayer. Indeed, the epilayer thickness W_{EP} must be analysed in relation with N_D, since the depletion depends on both parameters. In the inset of figure 4, we have represented the current as a function of the value of the peak electric field at the edge of the Schottky contact. Note that for a higher N_D, at a given applied voltage a higher electric field is achieved (as example, see circles in the inset of Figure 4, corresponding to an applied voltage of -5V). The vertical lines indicate the field at which the full depletion of the epilayer is observed in the simulations (not represented for N_D=6×10^{17} cm^{-3} since the breakdown appears when biasing below such condition). As expected, we have obtained similar values of the current as long as the epilayer is not fully depleted. However, once the epilayer is fully depleted, an increase of the current is observed. As a consequence, it is to note that for N_D=1 and 3×10^{17} cm^{-3} the diodes are not correctly designed (W_{EP}=350 nm is too small), since the current increase due to the epilayer depletion leads to a lowering of their breakdown voltage.

Figure 5 presents the *I-V* curves obtained from the simulations of diodes with the same doping level (N_D=6×10^{17} cm^{-3}) and without passivation (κ_{pas}=1), but with different epilayer thickness, together with the resulting current in a diode with N_D=10^{17} cm^{-3} and W_{EP}=2 µm. Note that for all of them the breakdown appears for voltages below the theoretical full depletion of the epilayer.

By comparison of the total current obtained for the diodes with W_{EP}=2 µm and different N_D, we confirm that, as expected, when reducing the doping, the breakdown voltage is significantly increased due to the lower electric field present at the contact for a given applied voltage and the associated smaller number of II processes taking place. The ratio between the current values obtained in the presence and in the absence of II processes in the simulation is represented in the inset of figure 5. For the highest doping (N_D=6×10^{17} cm^{-3}), there is an abrupt increase of this ratio near the breakdown voltage due to the stronger presence of II processes, while for the lowest doping the increase is smoother.

Ideally, within the full-depletion approximation, for a given doping level, the breakdown voltage should be the same regardless of the value of W_{EP} (as long as not all the epilayer is depleted). However, MC simulations show that 2D effects and the strong tunnel injection at the contact edge invalidate the full-depletion approximation, finally resulting in higher breakdown voltages for thicker epilayers. Thus, the largest diode (W_{EP}=2 µm) presents a higher breakdown voltage and, interestingly, it exhibits an increase of the current near the breakdown range which is less abrupt than for the smallest one (W_{EP}=350 nm).

Figure 6 shows the breakdown voltage as a function of the epilayer (a) doping and (b) thickness. It is found to decrease with increasing epilayer doping, figure 6(a), following a linear dependence according to the reported fitting, while it increases for thicker epilayer thickness, figure 6(b), in this

case with a quadratic dependence. These analytical expressions provide a simple way to quantify the observed trends and can serve as practical guidelines for device optimization.

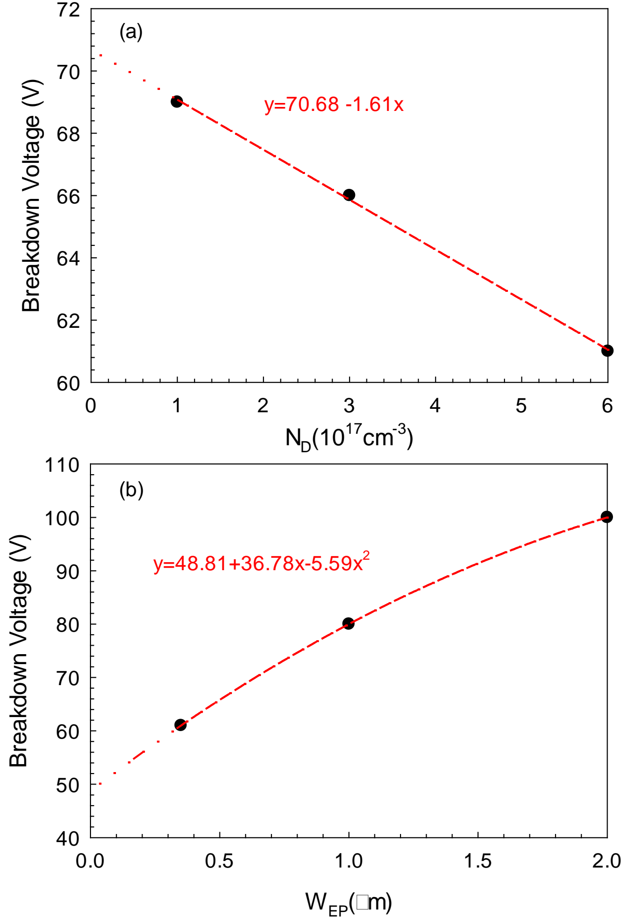

Figure 6. Breakdown voltage as a function of **(a)** the epilayer doping N_D for an epilayer thickness W_{EP}=350nm, **(b)** the epilayer thickness W_{EP} for an epilayer doping of N_D=6x10^{17} cm^{-3}. The lines correspond to the indicated analytical fittings.

Experimental values of breakdown voltage in GaN diodes with epilayer thickness and doping in the order of those considered here can be found in the literature. For example, Song et al. have employed a gradient doping technique in a 200 nm GaN drift layer to analyze the breakdown in different cases, obtaining a breakdown around 35 V for N_D=10^{17} cm^{-3} and 20 V for N_D=4x10^{17} cm^{-3} [30]. Liang et al. experimentally measured the breakdown voltage in GaN Schottky barrier diodes (W_{EP}= 200 nm and N_D= 5x10^{17} cm^{-3}), reporting values around 15 V [31]. Chen et al. demonstrated an improvement of the breakdown voltage (from 78 to 145 V) by applying a selective fluorine treatment in SBDs with W_{EP} =1 μm and N_D= 7x10^{16} cm^{-3} [32]. While the trends of the experimental values with N_D and W_{EP} are the same as those found in our simulations, the breakdown voltages obtained in this work are slightly higher than the experimental ones, as expected according to the quasi-ideal conditions considered here, since we are neglecting non-ideal leakage current mechanisms, like those related to traps, or the influence of dislocations.

To further analyze the behavior of the breakdown voltage, figure 7 shows the vertical profiles of electron (solid lines) and hole concentration (dashed lines) at the edge of the Schottky contact calculated for the largest diode (W_{EP}=2 μm) with two different doping levels and an applied voltage of -100 V. As observed in figure 5, this is practically the breakdown voltage for the diode with N_D=6×10^{17} cm^{-3}, while the avalanche is far for the diode with N_D=10^{17} cm^{-3}. For N_D=6×10^{17} cm^{-3}, the electron concentration (solid blue line) at the epilayer is even higher than the doping concentration. The electric field shows a sharp increase at the interface between the epilayer and the metal (taking values even above of the critical electric field, but along a very short length), originating a strong electron injection and intense II processes. The hole concentration is also extremely high throughout the epilayer, which indicates that the breakdown is originated by II events taking place all along the epilayer.

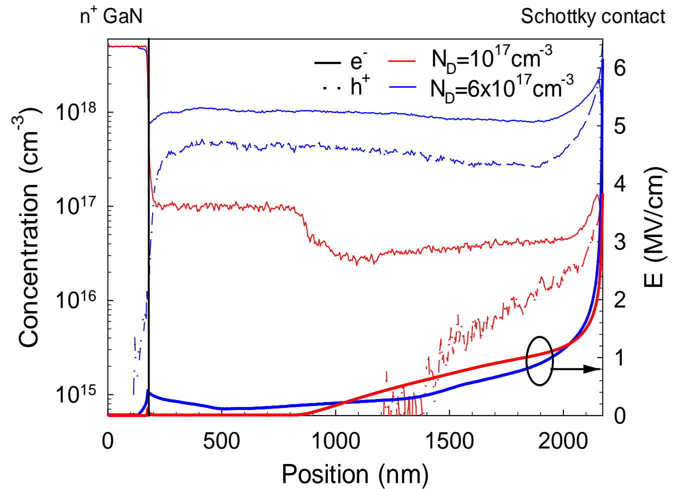

Figure 7. Vertical profiles of the electron (solid lines) and hole (dashed lines) concentration represented together with the electric field (thick lines) at the edge of the Schottky contact for N_D=10^{17} cm^{-3} (red) and 6x10^{17} cm^{-3} (blue) at V=-100 V.

On the other hand, the electron concentration corresponding to the diode with N_D=10^{17} cm^{-3} (solid red line) for this bias (still far from the breakdown) shows a partial depletion of the epilayer. Furthermore, as expected, the peak of the electric field at the interface is smaller than for N_D=6×10^{17} cm^{-3} and takes high values only in the depleted region. Thus, holes are present only near the Schottky contact, where II processes occur, and the hole concentration is lower. In summary, the key aspect which makes the difference when increasing the value of N_D is the enhanced tunnel injection (as a consequence of a narrower barrier) which leads to more frequent II events; the associated generation of holes further increasing the electron injection through the Schottky contact, thus leading the avalanche to take place at lower voltages.

The electric field as a function of the applied voltage V at three different positions of the Schottky contact (x=0, x=L_{Sch}/2 and x=L_{Sch}) is shown in figure 8 for the two diodes with N_D=6×10^{17} cm^{-3} studied above (W_{EP}=350 nm and 2 μm). For x=0 and x=L_{Sch}/2, the values of the electric field are similar. However, as expected, at the edge of the Schottky contact a higher electric field is obtained. For the largest diode (W_{EP}=2 μm), the electric field remains practically constant for |V|>40 V, while for the small diode (W_{EP}=350 nm) there is a sharp increase of the electric field near the breakdown voltage associated with onset of the increased hole concentration in the vicinity of the Schottky contact. Thus, the physical origin of the avalanche breakdown significantly depends on the 2D topology of the diode, particularly around the Schottky contact and its edge. In view of these results, the influence of L_{EP} is analyzed in the next section.

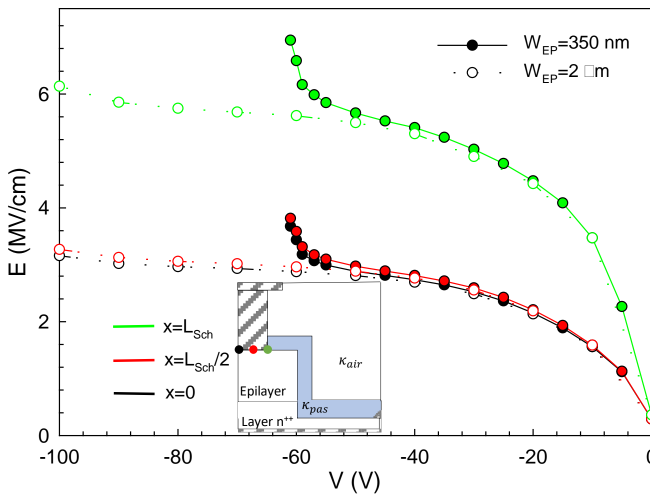

Figure 8. Electric field at the metal-semiconductor interface as a function of the voltage for two diodes with N_D=6x10^{17} cm^{-3}, L_{EP}=200 nm and different epilayer thickness: W_{EP}=350 nm (close circles) and 2 μm (open circles), calculated at three positions: x=0; x=L_{Sch}/2 and x=L_{Sch}. L_{Sch} =200 nm is the size of the Schottky contact. A scheme of the diode, where the positions are indicated, is included.

3.3 Epilayer Lateral Extension

Since the edge effects are extremely significant in the appearance of the avalanche breakdown, the epilayer lateral extension L_{EP} must be optimized. To this aim, diodes with N_D=6×10^{17} cm^{-3}, W_{EP}=2 μm and three different values of L_{EP} have been simulated. No passivation (κ_{pas}=1) is considered in these diodes. Note that this topology is not the optimal one, but it was selected because II effects are relevant enough to easily identify the influence of L_{EP}.

The *I-V* curves are represented in figure 9. Lower values of L_{EP} involve lower values of the current. In order to further evidence the importance of the 2D topology on the breakdown voltage, the *I-V* curve for the equivalent 1D structure (red rectangle of figure 1) has been included in the figure. As expected, the current is reduced with respect to the diodes with L_{EP}=100 nm and 200 nm, which can be explained by the absence of 2D effects (peak electric field at the contact edge). However, the current is higher than that obtained for a diode with L_{EP}=0 nm.

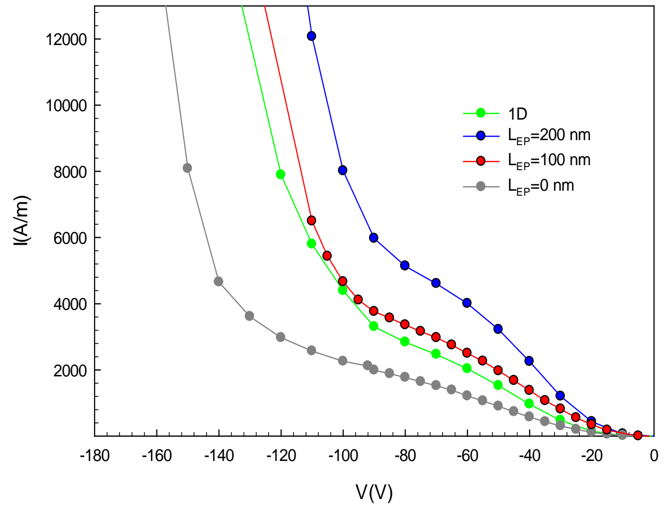

Figure 9. *I-V* curves obtained from the simulation of diodes with N_D=6x10^{17} cm^{-3}, W_{EP}=2 μm and different L_{EP}: 200 nm (blue), 100 nm (red) and 0 nm (grey). The *I-V* curve of a 1D vertical diode (green) with the same W_{EP}, N_D and L_{Sch} is also shown for comparison.

To illustrate this behavior, the MC profiles of electron and hole concentrations for V=-50 V are represented in figure 10 for the four considered diodes. The electron concentration near the Schottky contact is smaller when reducing L_{EP} due to the influence of the surface charge located at the vertical sidewall of the epilayer [18]. When the epilayer and the Schottky contact are aligned (L_{EP}=0 nm), the electron concentration dramatically decreases due to the depletion provoked by the surface charge. On the other hand, the hole concentration is higher for longer L_{EP} (200 nm), which is associated with a stronger tunnel injection due to the higher value of the vertical electric field at the contact edge. For L_{EP}=0 nm, the electric field is smaller due to the depletion, which is coherent with the lower injection.

In the 1D structure, quantities are uniform along the horizontal direction. As mentioned, interestingly, the current is higher than for the diode with L_{EP}=0 nm. The strong influence of the surface charge when L_{EP}=0 nm in the 2D structure reduces the current with respect to the 1D diode due to the lower electric field and consequently the lower tunnel injection and II events. Despite the depletion induced by the surface charges, the 2D cases with L_{EP}=100 and 200 nm provide a higher current than the 1D structure due to the higher electric field at the contact edge and the lateral extension beyond the contact where injected carriers can move along the vertical direction. Therefore, in order to optimize the design of these devices 2D simulations are

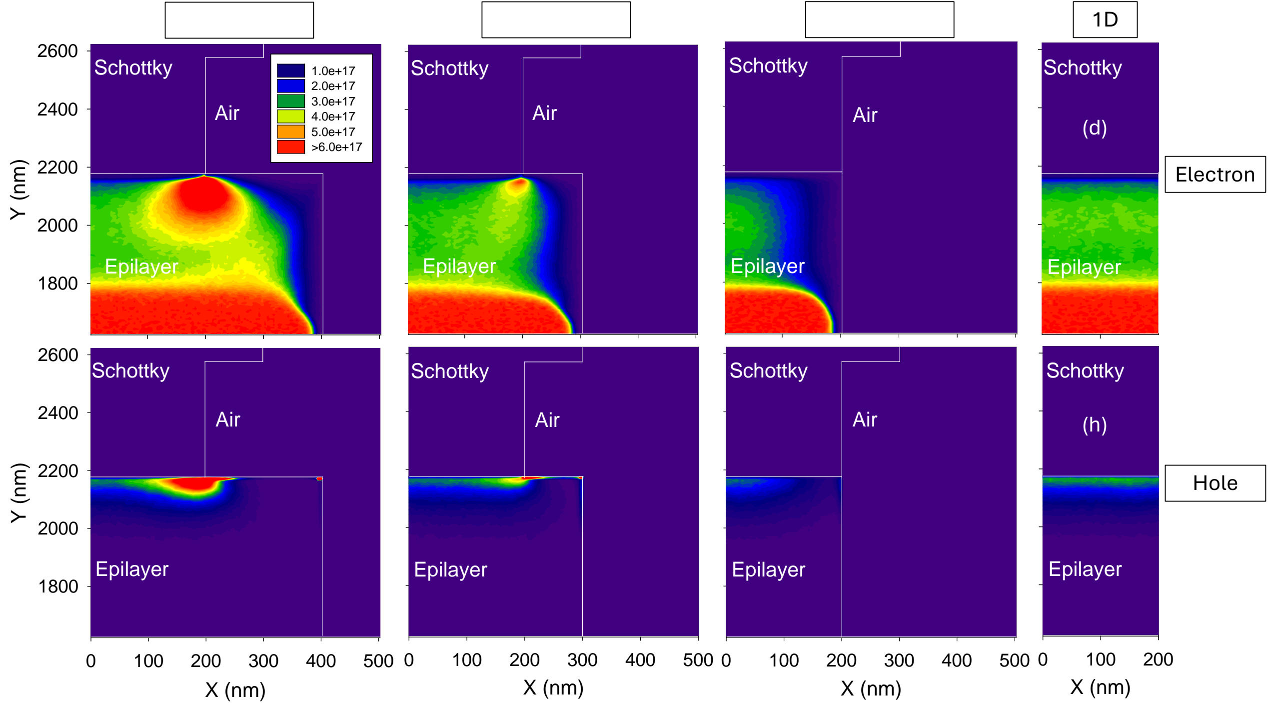

Figure 10. Colour maps for an epilayer with W_{EP}=2 μm and N_D=6x10^{17} cm^{-3} and an applied voltage of -50 V for **(a)** and **(e)** L_{EP}=200nm, **(b)** and **(f)** L_{EP}=100nm, **(c)** and **(g)** L_{EP}=0nm and **(d)** and **(h)** a 1D structure with the same contact length. **(a)**, **(b)**, **(c)** and **(d)** Electron and **(e)**, **(f)**, **(g)** and **(h)** hole concentration.

essential, indicating that higher breakdown voltages are reached in diodes with shorter L_{EP}.

In all the previous results, self-heating effects have been neglected. In small diodes like those analyzed here, the influence of the associated temperature rise is not found to be critical in the device breakdown, even if it could be slightly shifted to lower voltages. The temperature rise can be estimated by means of a thermal resistance (R_{th}) model. Considering a representative value of R_{th} of 300 K/W [33,34], a circular diode with a radius of 200 nm (the value of L_{Sch} considered here), a current level of 2500 A/m (around which the avalanche process starts in most of the simulated diodes) and an applied voltage of 60 V, the temperature rise is about 28 K, far from values leading to a thermal runaway or a significant current increase.

4. Conclusions

By means of 2D MC simulations, we have physically analyzed the influence of several technological parameters on the breakdown voltage of GaN SBDs originated by II. Under high reverse bias conditions, it is necessary to carefully consider tunnel injection and II events, since the positive feedback between these mechanisms leads to a significant increase of the carrier number ultimately provoking the breakdown of the diodes. A 2D modelling of the physical processes leading to the diode breakdown is essential for their correct description. In particular, the strong carrier injection taking place at the contact edge and the lateral depletion induced by the surface charges present at the semiconductor/dielectric interface require a 2D model to be correctly accounted for.

The results indicate that the passivation of the diodes is beneficial because lower values of electric field are reached at the contact edge the higher is the dielectric constant of the passivation material, leading to a lower tunnel injection, which may improve the breakdown voltage. The doping level and the thickness of the epilayer are key parameters for the improvement of the breakdown voltage. The thicker the epilayer and the lower the doping level, the higher the breakdown voltage, at the expense of a higher series resistance that may deteriorate the high-frequency performance of the SBDs. The optimum design should be the result of a trade-off between a good frequency performance and high breakdown voltage. Finally, a short lateral extension of the epilayer also helps to increase the breakdown voltage thanks to the reduction of the electric field at the contact edge induced by the surface charges at the semiconductor/dielectric interface; a self-aligned epilayer being the optimum design.

We remark that our analysis is qualitative, and some effects not considered in our model, like self-heating of the devices or trap-assisted tunneling, could modify the specific voltage values at which the breakdown takes place. But the observed tendencies and the conclusions reached about the influence of the different technological parameters remain valid as long as the breakdown is originated by II processes and tunneling. Moreover, other leakage-current mechanisms related to the

presence of traps, dislocations or defects may lead to breakdown voltages much lower than those predicted here.

TABLE II. SUMMARY OF DESIGN PARAMETERS INFLUENCING BREAKDOWN VOLTAGE

Parameter	Guideline	Trade-off
Passivation (κ_{pas})	High κ_{pas}	Increase of the edge effect capacitance
Doping level (N_D)	Low N_D	Higher series resistance
Epilayer thickness (W_{EP})	Thick epilayer	Higher series resistance
Epilayer lateral extension (L_{EP})	Self-aligned epilayer (L_{EP}=0)	Fabrication limit

Acknowledgements

This work has been partially supported through grants PID2023-147555OB-I00 and PDC2023-145896-I00 funded by MCIN/AEI/10.13039/501100011033, and the Junta de Castilla y León and FEDER through project SA136P23. The work of R. A. Peña was supported by the Junta de Castilla y León.

References

[1] Meneghini M., De Santi C., Abid I., Buffolo M., Cioni M., Abdul Khadar R., Nela L., Zagni N., Chini A., Medjdoub F., Meneghesso G., Verzellesi G., Zanoni E., Matioli E.: GaN-based power devices: Physics, reliability, and perspectives. J. Appl. Phys., 130 (18), 181101 (2021).

[2] Teo K. H., Zhang Y., Chowdhury N., Rakheja S., Ma R., Xie Q., Yagyu E., Yamanaka K., Li K., Palacios T.: Emerging GaN technologies for power, RF, digital, and quantum computing applications : Recent advances and prospects. J. Appl. Phys., 130 (16), 160902 (2021).

[3] Cuadrado-Calle D., Piironen P., Ayllon N.: Solid-state diode technology for millimeter and submillimeter-wave remote sensing applications: Current status and future trends. IEEE Microwave Magazine, 23 (6), 44–56 (2022).

[4] Mehdi I., Siles J. V., Lee C., Schlecht E.: THz diode technology: Status, prospects, and applications. Proc. IEEE, 105 (6), 990–1007 (2017).

[5] Siles J. V., Cooper K. B., Lee C., Lin R. H., Chattopadhyay G., Mehdi I.: A new generation of room-temperature frequency-multiplied sources with up to 10× Higher output power in the 160-GHz–1.6-THz range. IEEE Trans. THz Sci. Technol., 8 (6), 596-604 (2018).

[6] Maestrini A., Ward J. S., Tripon-Canseliet C., Gill J. J., Lee C., Javadi H., Chattopadhyay G., Mehdi I.: In-phase power-combined frequency triplers at 300 GHz. IEEE Microw. Wireless Compon. Lett., 18 (3), 218-220 (2008).

[7] Moro-Melgar D., Cojocari O., Oprea I., Hoefle M., Rickes M.: First generation of high-power discrete diodes based doublers beyond 300 GHz. Proc. Int. Symp. Space THz Technol., 1-4 (2018).

[8] Guo X., Zhong Y., Chen X., Zhou Y., Su S., Yan S., Liu J., Sun X., Sun Q., Yang H.: Reverse leakage and breakdown mechanisms of vertical GaN-on-Si Schottky barrier diodes with and without implanted termination. Appl. Phys. Lett., 118 (24), 243501 (2021).

[9] Di Gioia G., Frayssinet E., Samnouni M., Chinni V., Mondal P., Treuttel J., Wallart X., Zegaoui M., Ducournau G., Roelens Y., Cordier Y., Zaknoune M.: High Breakdown Voltage GaN Schottky Diodes for THz Frequency Multipliers. J. Electron. Mater., 52, 5249-5255 (2023).

[10] Orfao B., Abou Daher M., Peña R. A., Vasallo B. G., Pérez S., Íñiguez-de-la-Torre I., Paz-Martínez G., Mateos J., Roelens Y., Zaknoune M., González T.: Reverse-bias current hysteresis at low temperature in GaN Schottky barrier diodes. J. Appl. Phys., 135 (1), 014501 (2024).

[11] Fu K., Fu H., Huang X., Yang T., Cheng C., Peri P. R.: Reverse leakage analysis for as-grown and regrown vertical GaN-on-GaN Schottky barrier diodes. IEEE J. Electron Devices Soc., 8, 74-83 (2020).

[12] Guo X., Zhong Y., Chen X., Zhou Y., Su S., Yan S., Liu J., Sun X., Sun Q., Yang H.: Reverse leakage and breakdown mechanisms of vertical GaN-on-Si Schottky barrier diodes with and without implanted termination. Appl. Phys. Lett., 118 (24), 243501 (2021).

[13] Orfao B., Di Gioia G., Vasallo B. G., Pérez S., Mateos J., Roelens Y., Frayssinet E., Cordier Y., Zaknoune M., González T.: Comprehensive model for ideal reverse leakage current components in Schottky barrier diodes tested in GaN-on-SiC samples. J. Appl. Phys., 132 (4), 044502 (2022).

[14] Padovani F. A., Stratton R.: Field and thermionic-field emission in Schottky barriers. Solid State Electron., 9 (7), 695-707 (1966).

[15] Suda J., Yamaji K., Hayashi Y., Kimoto T., Shimoyama K., Namita H., Nagao S.: Nearly ideal current–voltage characteristics of Schottky barrier diodes formed on hydride-vapor-phase-epitaxy-grown GaN free-standing substrates. Appl. Phys. Express, 3 (10), 101003 (2010).

[16] Bandic Z. Z., Bridger P. M., Piquette E. C., McGill T. C., Vaudo R. P., Phanse V. M., Redwing J. M.: High voltage (450 V) GaN schottky rectifiers. Appl. Phys. Lett., 74 (9), 1266-1268 (1999).

[17] Li W., Nomoto K., Jena D., Xing H. G.: Thermionic emission or tunneling? The universal transition electric field for ideal Schottky reverse leakage current: A case study in β-Ga2O3. Appl. Phys. Lett., 117 (22), 222104 (2020).

[18] Orfao B., Vasallo B. G., Pérez S., Mateos J., Moro-Melgar D., Zaknoune M., González T.: Dielectric Passivation and Edge Effects in Planar GaN Schottky Barrier Diodes. IEEE Trans. Electron. Dev., 68 (9), 4296-4301 (2021).

[19] Liu X., Gu H., Li K., Wang J., Wang L., Kuo H. C., Liu W., Chen L., Fang J., Liu M., Lin X., Xu K., Ao J. P.: GaN Schottky barrier diodes on free-standing GaN wafer. ECS J. Solid State Sci. Technol., 6 (10), N216 (2017).

[20] Gonzalez T., Orfao B., Pérez S., Mateos J., Vasallo B. G.: Role of impact ionization and self-consistent tunnel injection in Schottky-barrier diodes operating under strong reverse-bias conditions. Appl. Phys. Express, 16 (2), 024003 (2023).

[21] Gonzalez T., Pardo D., Varani L., Reggiani L.: Monte Carlo analysis of noise spectra in Schottky-barrier diodes. Appl. Phys. Lett., 63 (22), 3040-3042 (1993).

[22] Pardo D., Grajal J., Pérez S., Mencía B., Mateos J., González T.: Analysis of noise spectra in GaAs and GaN Schottky barrier diodes. Semicond. Sci. Technol., 26 (5), 055023 (2011).
[23] Mott N. F., Sneddon I. N.: Wave Mechanics and its Applications. University Press, Oxford, 5 (2), 97 (1948).
[24] Moro-Melgar D., Mateos J., González T., Vasallo B. G.: Effect of tunnel injection through the Schottky gate on the static and noise behavior of GaInAs/AlInAs high electron mobility transistor. J. Appl. Phys., 116 (23), 1-7 (2014).
[25] Fowler R. H.: Statistical thermodynamics. CUP Archive (1939).
[26] Madelung O.: Semiconductors: data handbook. Springer-Verlag, New York (2004).
[27] García S., Pérez S., Íñiguez-de-la-Torre I., Mateos J., González T.: Comparative Monte Carlo analysis of InP-and GaN-based gunn diodes. J. Appl. Phys., 115 (4), 044510 (2014).
[28] Vasallo B. G., González T., Talbo V., Lechaux Y., Wichmann N., Bollaert S., Mateos J.: Impact ionization and band-to-band tunneling in $In_xGa_{1-x}As$ PIN ungated devices: A Monte Carlo analysis. J. Appl. Phys., 123 (3), 1–5 (2018).
[29] Chen S., Wang G.: High-field properties of carrier transport in bulk wurtzite GaN: A Monte Carlo perspective. J. Appl. Phys., 103 (2), 1–6 (2008).
[30] Song, X., Zhao, S., Dang, K., Yu, L., Zheng, M., Yao, Y., Zhang Y., Liu Z., Hao Y., Zhang, J.: 710 GHz GaN gradient doped Schottky barrier diode with high breakdown voltage. Appl. Phys. Lett., 126 (10), 103501 (2025).
[31] Liang, S., Song, X., Zhang, L., Lv, Y., Wang, Y., Wei, B., Guo Y., Gu G., Wang B., Cai S., Feng, Z.: A 177–183 GHz high-power GaN-based frequency doubler with over 200 mW output power. IEEE Electron Dev. Lett., 41 (5), 669-672 (2020).
[32] Chen, J., Bian, Z., Liu, Z., Ning, J., Duan, X., Zhao, S.,Wang H., Tang Q., Wu Y., Song Y., Zhang J., Hao, Y.: High-performance quasi-vertical GaN Schottky barrier diode with anode selective fluorine treatment. Semicond. Sci. Technol., 34 (11), 115019 (2019).
[33] Dong, Y., Liang, H., Liang, S., Zhou, H., Yu, J., Guo, H., Zeng H., Feng Z., Zhang, Y.: High-efficiency GaN frequency doubler based on thermal resistance analysis for continuous wave input. IEEE Trans. Electron Dev., 70 (9), 4565-4571 (2023).
[34] Górecki, P., Górecki, K., Kisiel, R., Myśliwiec, M.: Thermal parameters of monocrystalline GaN Schottky diodes. IEEE Trans. Electron Dev., 66 (5), 2132-2138 (2019).